PHYSICAL REVIEW E **88**, 041002(R) (2013)

Enhanced diffusion of nonswimmers in a three-dimensional bath of motile bacteria

Alys Jepson, Vincent A. Martinez, Jana Schwarz-Linek, Alexander Morozov, and Wilson C. K. Poon
SUPA, School of Physics & Astronomy, The University of Edinburgh, Mayfield Road, Edinburgh EH9 3JZ, United Kingdom
(Received 3 July 2013; published 28 October 2013)

We show, using differential dynamic microscopy, that the diffusivity of nonmotile cells in a three-dimensional (3D) population of motile *E. coli* is enhanced by an amount proportional to the active cell flux. While nonmotile mutants without flagella and mutants with paralyzed flagella have quite different thermal diffusivities and therefore hydrodynamic radii, their diffusivities are enhanced to the same extent by swimmers in the regime of cell densities explored here. Integrating the advective motion of nonswimmers caused by swimmers with finite persistence-length trajectories predicts our observations to within 2%, indicating that fluid entrainment is not relevant for diffusion enhancement in 3D.

DOI: 10.1103/PhysRevE.88.041002 PACS number(s): 47.63.Gd, 47.63.mf, 05.40.Jc

A collection of swimmers in a liquid (fish, motile algae, Janus colloids in "fuel", etc.) is an example of intrinsically nonequilibrium "active matter" [1], which show multiple intriguing activity-driven phenomena, e.g., novel pattern formation and counterintuitive rheology [2]. In particular, swimmers perturb the motion of passive species in their vicinity, from turning microgear wheels [3,4] to enhancing the motion of tracer colloids [5–10]. Understanding such phenomena is a challenge to statistical physics; it is also relevant biologically. Motile microorganisms live in the presence of and interact with nonswimmers of the same or different species, and nonliving debris such as food, substrates for colonization, etc. Such active-passive interactions are important ecologically [11], e.g., in cross-species predator-prey relationships.

The most well-studied active-passive mixture to date is colloids in a bacterial bath [5–9]. Experiments show that swimming bacteria enhance the long-time (nonthermal) diffusivity D of colloidal tracers linearly with the swimmer concentration [5] or, more generally, the active particle flux [6,7], $J_A = \bar{v} n_A$, where $\bar{v}$ and n_A are the average speed and number density of the swimmers, i.e.,

$$\Delta D = D - D_0 = \beta J_A, \tag{1}$$

with D_0 the (thermal) diffusivity in the absence of swimmers.

Significantly, all experiments supporting Eq. (1) [5–8] have been in two dimensions (2D), with the swimmers in a thin film [5] or close to one [6,7] or two [7,8] walls; in [5], the swimmers were at interacting concentrations. It remains unknown whether Eq. (1) holds under much simpler, bulk (3D) conditions far from any boundaries at low swimmer concentrations. Moreover, existing calculations [7] considering only far-field advection of tracer motion [12,13] significantly underestimate 2D observations [6,7]. One factor may be the presence of a range of swimmer-wall distances in the experiments. It has also been proposed recently [14] that advection and fluid entrainment [15] both contribute in 3D, but entrainment dominates in 2D. This theory predicts a value of β in 3D that is more than an order of magnitude larger than that given in [7].

Thus, the current situation, given in Table I, is far from satisfactory. To progress, confrontation of theory with 3D data is essential. We report a 3D study of enhanced diffusion in a bacterial bath using differential dynamic microscopy (DDM), which is uniquely able to deliver high-throughput 3D averaging [16]. We predict the measured β to within 2% by considering advection alone, showing that entrainment is negligible in 3D.

DDM measures the intermediate scattering function (ISF), $f(q,t)$, of a population of swimming *E. coli* [17], where q is the scattering vector and t is the time. Fitting the ISF gives the swimming speed distribution, and hence the average speed $\bar{v}$, the fraction of nonmotile organisms α, and the diffusivity of the nonmotile species D. The method has been validated in detail for wild-type (WT), i.e., run-and-tumble, and smooth swimming *E. coli* [18].

We use nonswimming cells as tracers. Since the fraction of motile organisms in as-prepared ("native") populations does not vary significantly from day to day, we add nonswimmers to native populations to study ΔD as a function of J_A. Thus, in general, there are three subpopulations in each of our samples: *native* motile (M) and nonmotile (N1) cells, and *added* nonmotile (N2) cells, with the latter being fluorescent and therefore distinguishable from native nonmotile cells. We performed DDM in phase contrast and fluorescence [19] modes, probing the motion of all the cells and only the diffusion of the added, fluorescent nonmotile mutants (N2), respectively.

K12-derived wild-type (WT) *E. coli* AB1157 and fluorescent nonmotile fliF (no flagella) or motA (paralyzed flagella) mutants [20] were grown and harvested as described before [18]. Suspensions at optical density OD = 0.5 (at 600 nm), corresponding to $7.8 \pm 0.2 \times 10^8$ cells/ml (=cell body volume fraction $\phi \approx 0.1\%$ based on cell volume of $V = 1.4 \pm 0.1\ \mu\text{m}^3$ [24]), were obtained by dilution.

DDM showed that as-prepared WT populations (M + N1) contained 20–40% native nonmotile (N1) cells (i.e., $\alpha =$ 0.6–0.8), and motile cells swam with $\bar{v} =$ 13–16 μm/s [17,18]. We studied the effect of $J_A = \bar{v} n_A = \bar{v}\alpha\phi/V$ on enhanced diffusion using three protocols. In most cases, we varied α directly by mixing WT and mutant cell suspensions at different ratios to obtain samples with fixed $\phi = 0.1\%$ and $\bar{v}$ in the narrow range $\bar{v} =$ 13–16 μm/s. To check that it is the combination $\bar{v}\alpha\phi$ that controls ΔD, we repeated these experiments but added glucose (0.006 wt%) into cell mixtures immediately before loading into capillaries, which increased $\bar{v}$ to $\lesssim$25 μm/s [25]. Finally, we studied a limited number of mixtures in which we varied ϕ at fixed α, or varied ϕ

TABLE I. Experiments (E) and theory (T) on tracer diffusion.

	Dimensionality	Effect(s) included	β (μm^4)[a]
E [7]	Next to wall		13 ± 0.7[b]
T [7]	Next to wall	Advection	2.0
T [7]	3D	Advection	0.48[c]
T [14]	3D	Advection + Entrainment	9.0
E [this work]	3D		7.1 ± 0.4
T [this work]	3D	Advection	7.24

[a]See Eq. (1) for the definition of β; cf. Fig. 2.
[b]Fitted value reported in [7] based on their Fig.8.
[c]Approximating swimmers as point dipoles, as in this work.

and α together. Taken together, these experiments accessed $0 \leqslant J_A \leqslant 14 \times 10^{-3}$ μm^{-2} s^{-1} by varying the component parameters of J_A in the range $0 \leqslant \alpha \lesssim 0.7$ and $0.04\% \lesssim \phi \lesssim 0.1\%$, and $\bar{v} \approx 15$ μm/s and ≈ 25 μm/s.

Observations began immediately after a glass capillary (depth 400 μm) was filled with ≈ 200 μl of solution and sealed with Vaseline to prevent drift. Forty-second-long phase-contrast movies (Nikon Plan Fluor 10× objective, NA = 0.3, 100 frame per second, 500^2 pixels) capturing all cells ($\sim 10^4$ M + N1 + N2), and fluorescence movies (Nikon Plan Fluor 20× objective with NA = 0.5, 20 fps, 1024^2 pixels excited at 450–490 nm) capturing only the added nonmotile mutants ($\sim 10^2$–10^3 N2), were consecutively recorded on an inverted microscope (Nikon TE300 Eclipse) with a Mikrotron high-speed camera (MC 1362) and frame grabber (Inspecta 5, 1 Gb memory). We image at 100 μm from the bottom of the capillary. This is significantly larger than the persistence length of WT *E. coli* (1 s run time $\equiv \lesssim$ 15–20 μm run length), so that they execute 3D motion. We have previously shown that the depth at 10× or 20× is large enough for DDM to return the 3D ISF of swimming *E. coli* [18].

Figure 1(a) shows ISFs from fluorescence DDM performed on a typical sample containing 70% WT cells (M + N1) and 30% motA mutants (N2) at a range of q values. Since only N2 cells fluoresce, the decay of these ISFs is exclusively due to the motion of the nonmotile motA mutants. The data collapse against $q^2\tau$, shown in Fig. 1(b), which means that their motion is well described as diffusive, and there is little evidence for non-Gaussianity [5,8,10] over our experimental window. As

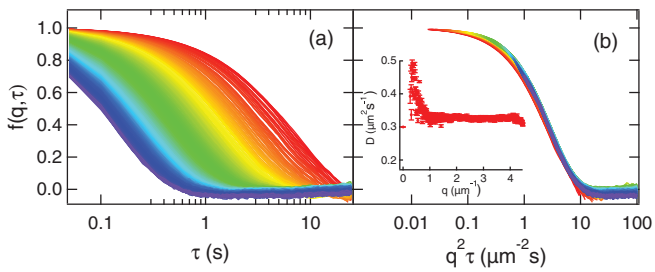

FIG. 1. (Color online) The ISF from fluorescence DDM of a sample at $\phi = 0.1\%$ with WT cells and motA mutants at a number ratio of 7:3 plotted against (a) τ and (b) $q^2\tau$. In each case, q increases from red to purple in a rainbow scale in the range $0.62 < q < 4.46$ μm^{-1}. The inset to (b) plots the fitted diffusivity of the nonmotile motA (N2) cells as a function of q.

a check, we plotted $\ln[w(q,\tau)]$ versus $\ln(\tau)$, where $w(q,\tau) = -\ln[f(q,\tau)]/q^2$ [26,27]. Only a hint of superdiffusion appears at very short times. The fitted values of D_{N_2} are shown as a function of q in the inset of Fig. 1(b). Averaging over the flat part of $D(q)$ ($1 \lesssim q \lesssim 3$ μm^{-1}) gives $\bar{D}_{N_2}^{(\mathrm{motA})} = 0.326 \pm 0.003$ μm^2/s. Repeating this procedure by mixing populations of native cells and nonmotile fliF or motA mutants, but always at a total $\phi = 0.1\%$, yields the dependence of D_{N_2} on n_A for each of the two different kinds of added motile cells, fliF and motA [Fig. 2(a), red], showing that ΔD increases linearly with n_A. In the same plot, we show data for swimmers in glucose with higher $\bar{v}$ (black). A linear dependence remains, but with a higher slope.

Before discussing diffusion enhancement, we first comment on the thermal diffusivity of various nonmotile cells. Measurements of fliF and motA mutants on their own [$J_A = 0$ in Fig. 2(a)] gave $D_{0,N2}^{(\mathrm{motA})} = 0.29 \pm 0.01$ μm^2/s and $D_{0,N2}^{(\mathrm{fliF})} = 0.39 \pm 0.01$ μm^2/s $\approx 1.4 \times D_{0,N2}^{(\mathrm{motA})}$. This is consistent with tracking measurements [28], which found that deflagellated cells diffused $\approx 50\%$ faster than cells with paralyzed flagella. The unenhanced diffusivity of native nonmotile cells (N1) cannot be accessed directly, but can be obtained by performing DDM on more and more dilute suspensions of AB1157 (i.e., using a native mixture of M + N1 cells and taking the limit $J_A \to 0$), from which we found $D_{0,N1} = 0.37 \pm 0.02$ μm^2/s. This value is, within uncertainties, the same as that of the fliF mutants, suggesting that nonmotile WT cells probably have had their flagella sheared off during preparation. Indeed, DDM measurements showed that gentler preparative protocols (e.g., using blunted pipette tips to reduce shear) generally increased the motile fraction α.

Returning to diffusivity enhancement, we find that all four data sets in Fig. 2(a) collapse onto a universal line if we plot the change in diffusivity, $\Delta D_{N2} = D_{N2} - D_{0,N2}$, versus the swimmer flux, J_A; see Fig. 2(b). All the data in Fig. 2(a) were obtained at fixed overall cell concentration $\phi = 0.1\%$. Figure 2(b) includes data points in which J_A is varied by changing ϕ (green points) or by changing ϕ and α together (blue points). These also fit into the universal linear dependence within experimental errors. Thus, $J_A = \bar{v}\alpha\phi/V$ is indeed the operative variable in controlling diffusion enhancement: $\Delta D_{N2} = \beta J_A$, with the best-fit value of $\beta = 7.1 \pm 0.4$ μm^4.

An implicit assumption so far has been that the diffusivity of each nonswimmer is enhanced *independently*. Figure 2(b) includes experiments performed over $0.04\% \lesssim \phi \lesssim 0.1\%$,

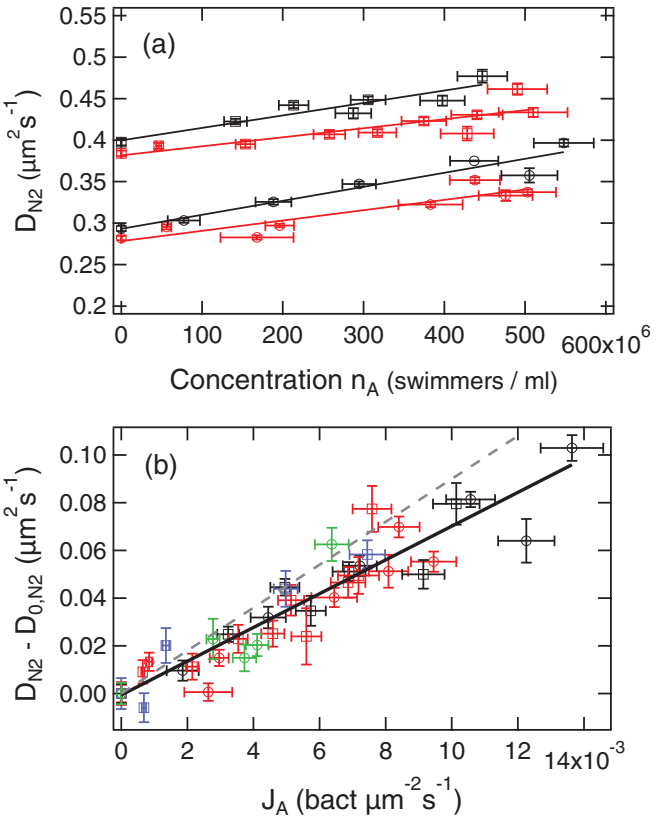

FIG. 2. (Color online) (a) Effective diffusivity D_{N2} of motA (circles) and fliF (squares) in suspensions of *E. coli* AB1157 containing no glucose (red, $\bar{v} = 13$–16 μm/s) or containing glucose (black, $\bar{v} \lesssim 25$ μm/s), while α is varied at a fixed total cell density $\phi = 0.1\%$, with best-fit lines. (b) The same data plotted as diffusivity enhancement $\Delta D = D_{N2} - D_{0,N2}$ for both motA and fliF data sets with and without glucose vs the active particle flux, $J_A = \bar{v} n_A = \bar{v}\alpha\phi/V$. Green and blue points: data taken by varying ϕ or by varying both ϕ and α. Equation (1) fitted through all points gives $\beta = 7.1 \pm 0.4$ μm^4. Dashed line: prediction of [14]. All error bars give $\pm$ standard deviation.

$0 < \alpha \lesssim 0.7$, giving in each case a volume fraction of $(1-\alpha)\phi$ of nonmotile cells (N1 or N1 + N2). The observed data collapse is consistent with little or no interaction between the nonswimmers. We checked this directly by measuring the diffusivity of fliF or motA cells on their own at $\phi = 0.01\%$ and $\phi = 0.1\%$, and found no change within experimental errors.

Equation (1) has been demonstrated before in 2D [6,7]. In a bath of *E. coli* and 2 μm beads between two glass walls separated by $h = 20$ μm, tracking gave $\beta \approx 45$ μm^4, dropping to ≈ 10 μm^4 for $h = 110$ μm, where bacteria and tracers remain close to one wall, so that surface effects still dominate. Our bulk value of $\beta \approx 7$ μm^4 is smaller than any of these values [29].

Significantly, although motA and fliF have different thermal diffusivities (and therefore hydrodynamic radii), their motion is enhanced to the same extent (same β); see Fig. 2(b). Previously, enhancement in 2D close to a wall was found to be the same for 1 and 2 μm tracers [6]. These findings recall particle imaging velocimetry (PIV), where small tracers sufficiently close to being neutrally buoyant follow the streamlines in a flow field. Corrections due to finite tracer size (radius R) scale as $(R/\ell)^2$ according to Faxén's law [30], for an average swimmer-tracer distance ℓ. The "PIV regime" is obtained if $(R/\ell)^2 \ll 1$.

To estimate ℓ, we approximate swimming *E. coli* cells by equivalent-volume spheres of diameter $d \approx 1.4$ μm, so that $\ell \sim d\phi^{-1/3} \approx 14$ μm at our highest total cell concentration ($\phi \approx 10^{-3}$). For native nonswimmers and fliF mutants without flagella, we take $2R = d \approx 1.4$ μm, so that $(R/\ell)^2 \approx 0.003$. Thus, we are in the PIV regime as in previous work using 1–2 μm colloidal tracers [6]. However, for motA mutants with $\lesssim 10$ μm paralyzed flagella, $(R/\ell)^2 \lesssim 0.5$. Thus, at ϕ somewhat higher than our highest value, motA mutants will be out of the PIV regime; the physics in this case remains to be explored.

A tracer near a passing swimmer executes a not-quite-closed loop [7,12,13,15] due to far-field fluid advection, resulting in a net displacement. We adapt a theory developed for "squirmers" [13] to *E. coli* [31], and show that integrating these motions over bacterial trajectories with finite persistence length accurately explains our data.

Each flagellated *E. coli* cell is a pusher; the far-field fluid velocity at a distance $\mathbf{r}$ from a cell is dipolar [32]:

$$\mathbf{v}(\mathbf{r}) = \frac{p\,\mathbf{r}}{r^3}[3\cos^2\theta - 1], \tag{2}$$

with strength $p = kv$, v the swimming speed, and k a geometric constant with dimensions (length)^2. We model WT cells using particles that swim straight over a persistence length λ before randomly changing direction.

The total displacement of a tracer is the sum of many "elementary scattering events", each of which is characterized by two "impact parameters": the distance a from the tracer and the distance b from the start of the straight trajectory, to the point of the closest approach; see Fig. 3. If $\lambda \to \infty$, such scattering events result in closed or almost-closed loop trajectories of the tracer [7,12,13,15] and a slightly enhanced tracer diffusivity. Real swimmers have finite λ, so that tracers only execute parts of these looplike trajectories, giving larger net displacements during each scattering event and higher ΔD [13].

The mean-squared displacement of a tracer $\langle|\mathbf{x}(t)|^2\rangle$ comes from summing individual displacements $\delta(a,b)$ over all

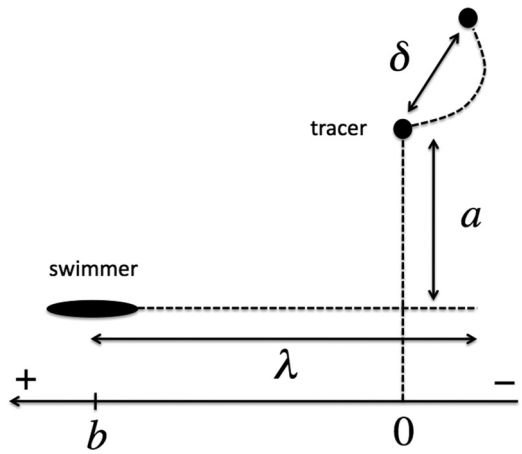

FIG. 3. Schematic of an "elementary scattering event" between a swimmer and a tracer. See text for definition of symbols.

possible scattering configurations a and b. Assuming identical, noninteracting, isotropic swimmers and statistically independent events [13]:

$$\langle|\mathbf{x}(t)|^2\rangle \equiv 6\Delta D t = \left(\frac{2\pi n_A v t}{\lambda}\right)\int_0^\infty\int_{-\infty}^\infty a\delta^2(a,b)dbda. \quad (3)$$

To understand the prefactor (...), note that in time t, each swimmer "tumbles" $v\,t/\lambda$ times to give $n_A\,v\,t/\lambda$ scattering events of the type shown in Fig. 3. To evaluate Eq. (3), we numerically integrate the tracer equations of motion, $\dot{\mathbf{r}}_t(t) = \mathbf{v}[\mathbf{r}_t(t) - \mathbf{r}_s(t)]$, where $\mathbf{r}_t(t)$ and $\mathbf{r}_s(t) = \mathbf{r}_s(0) + v\,t\,\hat{\mathbf{e}}$ are the positions of the tracer and swimmer, respectively. The initial position and swimming direction $\hat{\mathbf{e}}$ are set by the scattering parameters a and b. Repeating for sets of (a,b) and summing up the resulting displacements, we find an enhanced diffusivity for the dipolar pusher velocity field [Eq. (2)]:

$$\Delta D = 3.44\,n_A\,v\left(\frac{p}{v}\right)^2 = 3.44k^2J_A. \quad (4)$$

Detailed calculations [31] show that, as for squirmers [13], the numerical prefactor in Eq. (4) is not very sensitive to the range of (λ,p,v) relevant for swimming *E. coli* [32], for which $k = 1.45\ \mu\text{m}^2$, and Eq. (4) predicts $\Delta D = \beta J_A$ with $\beta = 7.24\ \mu\text{m}^4$, in remarkably good agreement with our value (Fig. 2) of $\beta = 7.1 \pm 0.4\ \mu\text{m}^4$.

Previous calculations at $\lambda \to \infty$ give $\beta = 0.48\ \mu\text{m}^4$ [7] because, here, tracers execute almost-closed loops [12]. For finite λ, the largest contribution to the integral in Eq. (3) comes from $b = 0$ and $b = \lambda$ [13]. At these scattering events (Fig. 3), a swimmer starting or finishing at the point of closest approach causes a tracer to perform approximately half of the infinite-λ almost-closed loop, giving significantly larger total displacements. Indeed, preliminary DDM measurements using a smooth swimming mutant, which has a significantly higher λ than a run-and-tumble swimmer, showed lower enhanced diffusion of the nonswimmers.

To summarize, we have observed that the enhanced diffusion of nonmotile cells in a 3D bath of motile *E. coli* scales linearly with the motile cell flux (Fig. 2). The scaling is accurately accounted for by summing tracer displacements due to far-field advection induced by individual swimmers with long but finite persistence-length trajectories. Interestingly, it has been recently suggested [14] that fluid entrainment is also important, which, together with advection, give $\beta = 9\ \mu\text{m}^4$ in 3D, which is a value incompatible with our observations [Fig. 2(b)] [33].

We have worked at $\phi \lesssim 0.1\%$, where the diffusivities of nonmotile fliF and motA mutants are enhanced equally. At higher ϕ, this situation should change because motA cells with paralyzed flagella are then too large to be considered tracers. Separately, it should be interesting to probe concentrated systems in which the density of tracers is increased until they interact with each other.

A.J., V.A.M., A.N.M., and W.C.K.P. were funded by an EPSRC studentship, Grants No. EU FP7-PEOPLE (PIIF-GA-2010-276190), No. EPSRC EP/I004262/1, and No. EPSRC EP/J007404/1, respectively. We thank G. Dorken for assisting with plasmid transformations and M. E. Cates, E. Clément, G. Miño, and D. Pushkin for discussions.

[1] S. Ramaswamy, Annu. Rev. Condens. Matter Phys. **1**, 323 (2010).
[2] M. E. Cates, Rep. Prog. Phys. **75**, 042601 (2012).
[3] A. Sokolov, M. M. Apodaca, B. A. Grzybowski, and I. S. Aranson, Proc. Natl. Acad. Sci. USA **107**, 969 (2010).
[4] L. Angelani, R. Di Leonardo, and G. Ruocco, Phys. Rev. Lett. **102**, 048104 (2009).
[5] X. L. Wu and A. Libchaber, Phys. Rev. Lett. **84**, 3017 (2000).
[6] G. L. Miño, T. E. Mallouk, T. Darnige, M. Hoyos, J. Dauchet, J. Dunstan, R. Soto, Y. Wang, A. Rousselet, and E. Clément, Phys. Rev. Lett. **106**, 048102 (2011).
[7] G. L. Miño, J. Dunstan, A. Rousselet, E. Clément, and R. Soto, J. Fluid Mech. **729**, 423 (2013).
[8] C. Valeriani, M. Li, J. Novosel, J. Arlt, and D. Marenduzzo, Soft Matter **7**, 5228 (2011).
[9] D. T. N. Chen, A. W. C. Lau, L. A. Hough, M. F. Islam, M. Goulian, T. C. Lubensky, and A. G. Yodh, Phys. Rev. Lett. **99**, 148302 (2007).
[10] K. C. Leptos, J. S. Guasto, J. P. Gollub, A. I. Pesci, and R. E. Goldstein, Phys. Rev. Lett. **103**, 198103 (2009).
[11] H. Grossart, L. Riemann, and F. Azam, Aquat. Microb. Ecol. **25**, 247 (2001).
[12] J. Dunkel, V. B. Putz, I. M. Zaid, and J. M. Yeomans, Soft Matter **6**, 4268 (2010).
[13] Z. Lin, J. L. Thiffeaul, and S. Childress, J. Fluid Mech. **669**, 167 (2011).
[14] D. O. Pushkin and J. M. Yeomans, arXiv:1307.6025v1.
[15] D. O. Pushkin, H. Shum, and J. M. Yeomans, J. Fluid Mech. **726**, 5 (2013).
[16] R. Cerbino and V. Trappe, Phys. Rev. Lett. **100**, 188102 (2008).
[17] L. G. Wilson, V. A. Martinez, J. Schwarz-Linek, J. Tailleur, G. Bryant, P. N. Pussey, and W. C. K. Poon, Phys. Rev. Lett. **106**, 018101 (2011).
[18] V. A. Martinez, R. Besseling, O. A. Croze, J. Tailleur, M. Reufer, J. Schwarz-Linek, L. G. Wilson, M. A. Bees, and W. C. K. Poon, Biophys. J. **103**, 1637 (2012).
[19] P. J. Lu, F. Giavazzi, T. E. Angelini, E. Zaccarelli, F. Jargstorff, A. B. Schofield, J. N. Wilking, M. B. Romanowsky, D. A. Weitz, and R. Cerbino, Phys. Rev. Lett. **108**, 218103 (2012).
[20] Step 1 in flagellar synthesis in fliF [21] and synthesis of the stator complex in the motor in motA [22] are disrupted. Fluorescence comes from inclusion of the Green Fluorescent Protein-encoding plasmid pHC60 [23].
[21] H. Terashima, S. Kojima, and M. Homma, Int. Rev. Cell. Mol. Biol. **270**, 39 (2008).
[22] G. E. Dean, R. M. Macnab, J. Stader, P. Matsumura, and C. Burks, J. Bacteriol. **159**, 991 (1984).
[23] H. P. Cheng and G. C. Walker, J. Bacteriol. **180**, 5183 (1998).

[24] From measuring 60 cells using $\times 100$ phase-contrast microscopy.
[25] J. Adler and B. Templeton, J. Gen. Microbiol. **46**, 175 (1967).
[26] V. A. Martinez, G. Bryant, and W. van Megen, Phys. Rev. Lett. **101**, 135702 (2008).
[27] V. A. Martinez, J. H. J. Thijssen, F. Zontone, W. van Megen, and G. Bryant, J. Chem. Phys. **134**, 054505 (2011).
[28] S. Tavaddod, M. Charsooghi, F. Abdi, H. Khalesifard, and R. Golestanian, Eur. Phys. J. E **34**, 1 (2011).
[29] Cell densities in [5] were $\sim 10^2\times$ those used here or in [6,7]; the data cannot be compared directly.
[30] J. Happel and H. Brenner, *Low Reynolds Number Hydrodynamics* (Prentice-Hall, Englewood Cliffs, NJ, 1965).
[31] A. Morozov and D. Marenduzzo, arXiv:1308.3387.
[32] K. Drescher, J. Dunkel, L. H. Cisneros, S. Ganguly, and R. E. Goldstein, Proc. Natl. Acad. Sci. USA **108**, 10940 (2011).
[33] Note, however, that [14] predicts $\beta = 7.6\ \mu\mathrm{m}^4$ for 3D advection alone, consistent with our work.